nature climate change

ARTICLES

https://doi.org/10.1038/s41558-021-01157-9

Double benefit of limiting global warming for tropical cyclone exposure

Tobias Geiger[1,2]✉, Johannes Gütschow[1], David N. Bresch[3,4], Kerry Emanuel[5] and Katja Frieler[1]

Tropical cyclone (TC) impacts are expected to worsen under continued global warming and socio-economic development. Here we combine TC simulations with an impact model to quantify country-level population exposure to TC winds for different magnitudes of global mean surface temperature increase and future population distributions. We estimate an annual global TC exposure increase of 26% (33 million people) for a 1 °C increase in global mean surface temperature, assuming present-day population. The timing of warming matters when additionally accounting for population change, with global population projected to peak around mid-century and decline thereafter. A middle-of-the-road socio-economic scenario combined with 2 °C of warming around 2050 increases exposure by 41% (52 million). A stronger mitigation scenario reaching 2 °C around 2100 limits this increase to 20% (25 million). Rapid climate action therefore avoids interference with peak global population timing and limits climate-change-driven exposure. Cumulatively, over 1.8 billion people could be saved by 2100.

Tropical cyclones (TCs) expose 150 million people annually[1], cause tremendous damage and interrupt economies in the long run[2]. TC impacts (or risks) emerge through the interplay of the TC hazard, the exposure of goods or people to this hazard, and the specific vulnerability of exposed people, infrastructure and environment[3]. Historically, climate change[4], socio-economic development[1] and respective changes in vulnerability[5,6] have contributed to the rise in TC impacts. In the future, TC impacts are expected to worsen further through the harmful interference of the climate-change-driven increase in TCs of the highest category[7] and socio-economic development[8] in exposed coastal urban areas[9]. Further compounding may occur through increasing co-hazards such as extreme precipitation[10], stalling events[11] and stronger surges due to sea level rise[12], as well as through general maladaptation practices[6] and poleward-shifted landfalls to previously non-disaster-prone and therefore less prepared regions[13]. So far, a rigorous quantification of future TC exposure is missing. Research has mostly focused on projected changes in physical TC properties (for example, changes in the TC power dissipation index[14]) or on single-country[15] or global but general impact assessments[16,17].

Here we conduct a globally consistent, regionally calibrated, country-specific assessment of population exposed to TC winds under socio-economic development and climate change, which presently available TC models are not designed for or are computationally incapable of conducting. The quantification of the population exposed to severe winds additionally provides an essential contribution to understanding and estimating related future direct impacts (for example, fatalities or damages) and indirect impacts (for example, on economic development[18]). Our present assessment is based on novel TC simulations from the latest round of the Inter-sectoral Impact Model Intercomparison Project (ISIMIP2b)[19], using a well-established TC model[14] and the impact model CLIMADA[20]. The TC simulations comprise 642,000 tracks for 2,140 modelling years driven by the output from four general circulation models (GCMs), available for the historical and future periods for two different representative concentration pathways (RCPs): RCP2.6 and RCP6.0 (see Methods for the details). The available TC simulations are post-processed by a probabilistic tool that first analyses how TC frequency (defined as the number of TC landfalls per year) and TC intensity vary with global mean surface temperature (GMST) change and large-scale patterns of internal variability such as the El Niño/Southern Oscillation (ENSO). Second, large numbers of random TC samples are created that mimic the number of TC landfalls and mean landfall intensity in a given region and year (see Methods for details on the tool). The tool is thus able to comprehensively sample the uncertainty in exposure that arises through the stochastic process of actual landfall location, which greatly varies (in terms of socio-economic consequences) for landfalls in rural areas or densely populated megacities. This tool further allows one to study TC impacts under socio-economic development and various global warming pathways that are not captured by the GCMs—for example, the warming pathway according to the Nationally Determined Contributions (NDCs)[21] considered later.

Results

We first fix population patterns at 2015 values and analyse trends in population exposure as a function of GMST only (Fig. 1). We define a person to be exposed to TC winds if this person experiences one-minute sustained hurricane-force winds (≥64 knots), regardless of the actual landfall of the TC's centre. To quantify exposure, we overlay population maps for the historical[22] and future[23] periods with the same spatial resolution of 0.1 degree (approximately 11 km at the Equator). We observe large fluctuations in observed and modelled exposure. Interannually, the number of exposed people can vary by more than 100 million due to TCs affecting densely or sparsely populated areas and uncertainty considerations of the probabilistic tool (see Methods for the details). Although the probabilistic tool is uncalibrated with respect to exposure, we

[1]Potsdam Institute for Climate Impact Research (PIK), Member of the Leibniz Association, Potsdam, Germany. [2]Deutscher Wetterdienst (DWD), Climate and Environment Consultancy, Stahnsdorf, Germany. [3]Institute for Environmental Decisions, ETH Zurich, Zurich, Switzerland. [4]Federal Office of Meteorology and Climatology MeteoSwiss, Zurich-Airport, Switzerland. [5]Program in Atmospheres, Oceans and Climate, Department of Earth, Atmospheric and Planetary Sciences, Massachusetts Institute of Technology, Cambridge, MA, USA. ✉e-mail: geiger@pik-potsdam.de

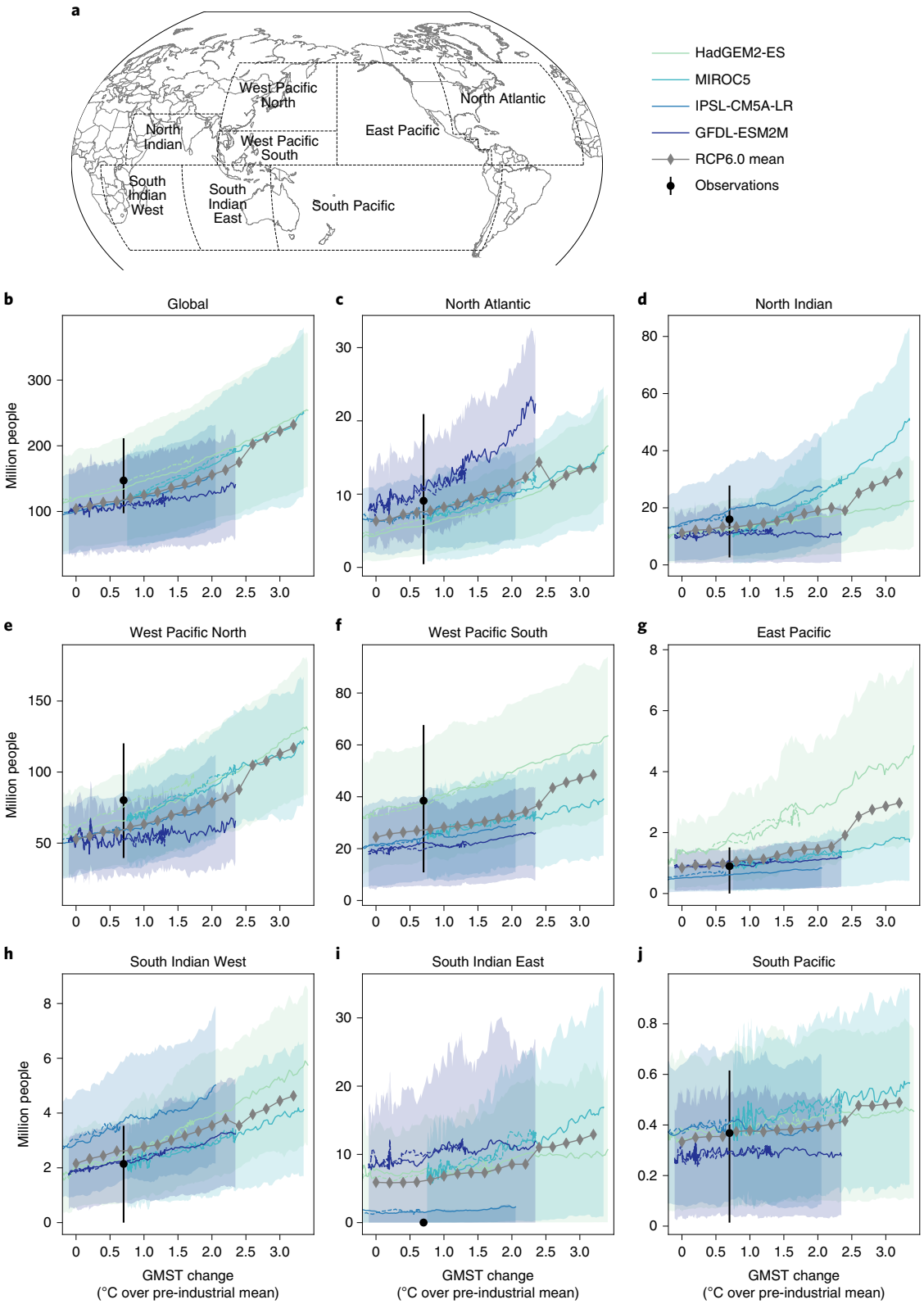

Fig. 1 | Increase in annual population exposure with GMST. a, Region definitions. **b**–**j**, Modelled GCM-specific (colours) and RCP-specific (dashed lines for RCP2.6; solid lines for RCP6.0) global (**b**) and regional (**c**–**j**) population exposed to TC wind speeds of at least 64 knots for fixed 2015 population patterns as a function of GMST change with respect to the observed 1850–1900 pre-industrial GMST mean. The colour shading (for RCP6.0 only) indicates the 66.7% confidence intervals around the 11-year running GCM-specific mean values; the grey solid line is the GCM mean under RCP6.0 binned at 0.2 °C intervals. Historical exposure (black dots, 1980–2015 mean) with 66.7% percentile interannual variability is positioned at the 1980–2015 mean warming level (0.7 °C). Note that GCM-specific scaling of exposure is almost identical for different RCPs such that RCP2.6 and RCP6.0 lines might coincide. The uncertainty assessment for modelled exposure is based on 1,712,000 TC samples, obtained by drawing 100 artificial TC seasons for each basin, GCM, warming scenario and year.

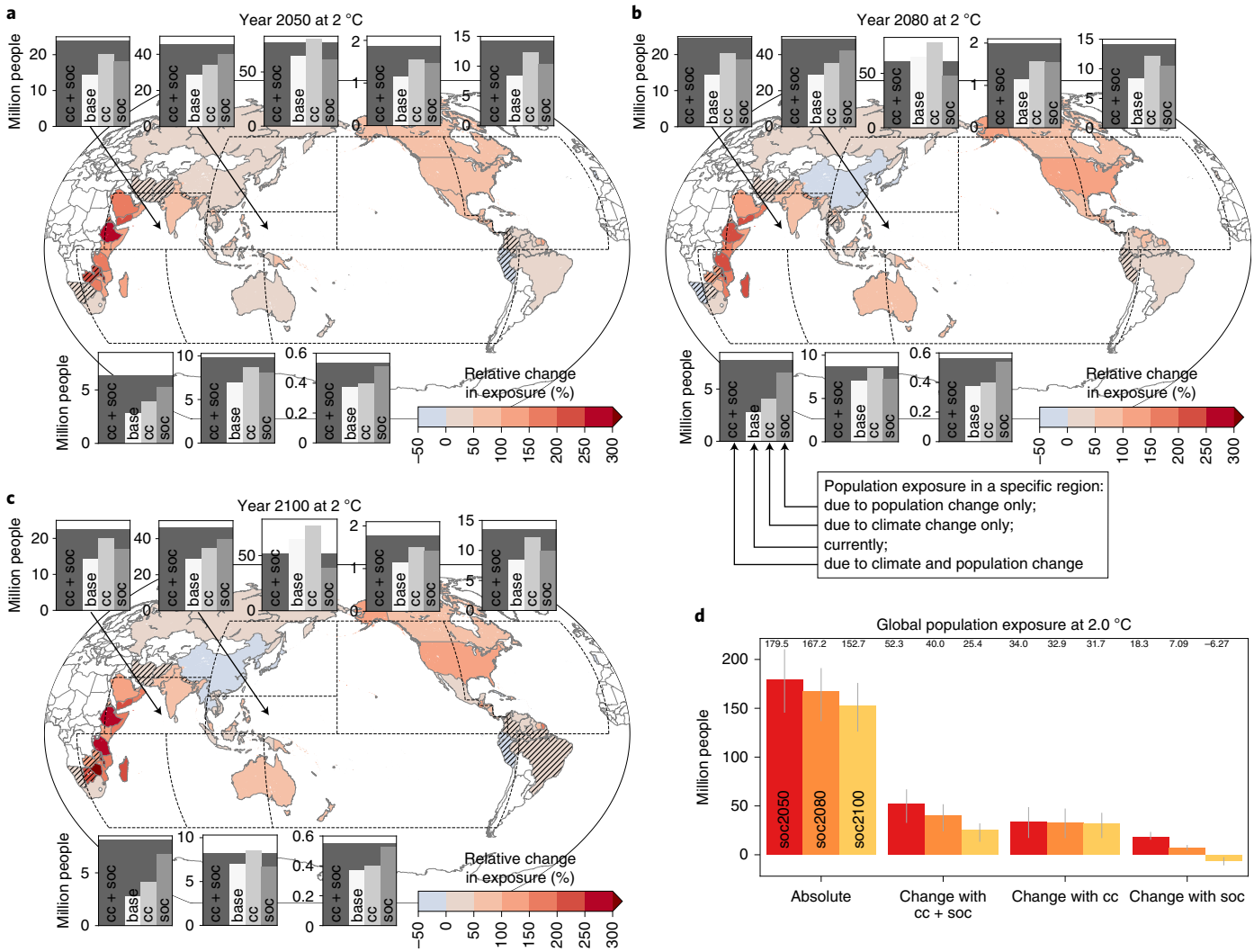

Fig. 2 | Population exposure for different base years of socio-economic development and 2 °C of warming. a–c, Maps displaying the mean relative change in country-specific population exposure between the baseline (2015, 1 °C) and 2 °C of warming for different base years (2050, **a**; 2080, **b**; and 2100, **c**) under socio-economic development according to SSP2. Hatching indicates countries where fewer than three model realizations agree on the sign of the change. The map insets show modelled absolute population exposure (in millions of people) for eight different regions separated by drivers of change (base, 1 °C warming with 2015 population patterns; cc, 2 °C warming with 2015 population patterns; soc, 1 °C warming with SSP2-based population patterns; cc + soc, 2 °C warming with SSP2-based population patterns). **d**, Globally aggregated absolute exposure and exposure change with respect to the baseline separated into the drivers of change for different base years (2050, red; 2080, orange; and 2100, yellow). The whiskers indicate the exposure range due to the different model realizations.

find good agreement between observations and the model. On the global scale, simulated annual mean exposure is underestimated with respect to observations but lies well within uncertainty ranges (Fig. 1b). In addition to the annual mean values, we verified that the simulated distribution of the annually exposed population agrees well with observations (Extended Data Fig. 1). In absolute terms, about three-quarters of the globally exposed population reside around the western Pacific (Fig. 1e,f). The western Pacific is also the region where observed exposure is higher than modelled exposure, while the opposite is true in the southeastern Indian Ocean (Fig. 1i). In all other world regions, the multi-GCM mean agrees very well with observed exposure. When comparing observed and simulated exposure, one has to be cautious of the statistical subtleties involved. While our tool allows for the creation of hundreds of simulated samples (100 artificial TC seasons per GCM, basin and year), there is only a single and random realization of observed exposure to compare with. Given the large interannual variability of observed exposure caused by seasonal activity and the stochastic process of landfall location (Fig. 1), the validation of our tool in terms of exposure is limited (see Methods for further details).

Irrespective of the underlying GCM driving the TC simulation, we observe an increase in modelled population exposed to TCs due to global warming. The multi-GCM long-term mean between 1 °C and 2 °C GMST change projects an increase in population exposure by more than 30 million people at fixed 2015 population patterns. This trend is almost independent of the underlying RCP scenario associated with different rates of warming (solid and dashed lines in Fig. 1). The trends in TC exposure under global warming are GCM-specific and region-specific and are caused by varying changes in TC frequency and intensity (Supplementary Tables 1 and 2). When artificially fixing simulated TC frequency at the current levels (1 °C of warming), we observe a slowdown in population exposure to about 8 million people per degree of warming, driven by a diverse response across basins and GCMs (Extended Data Fig. 2).

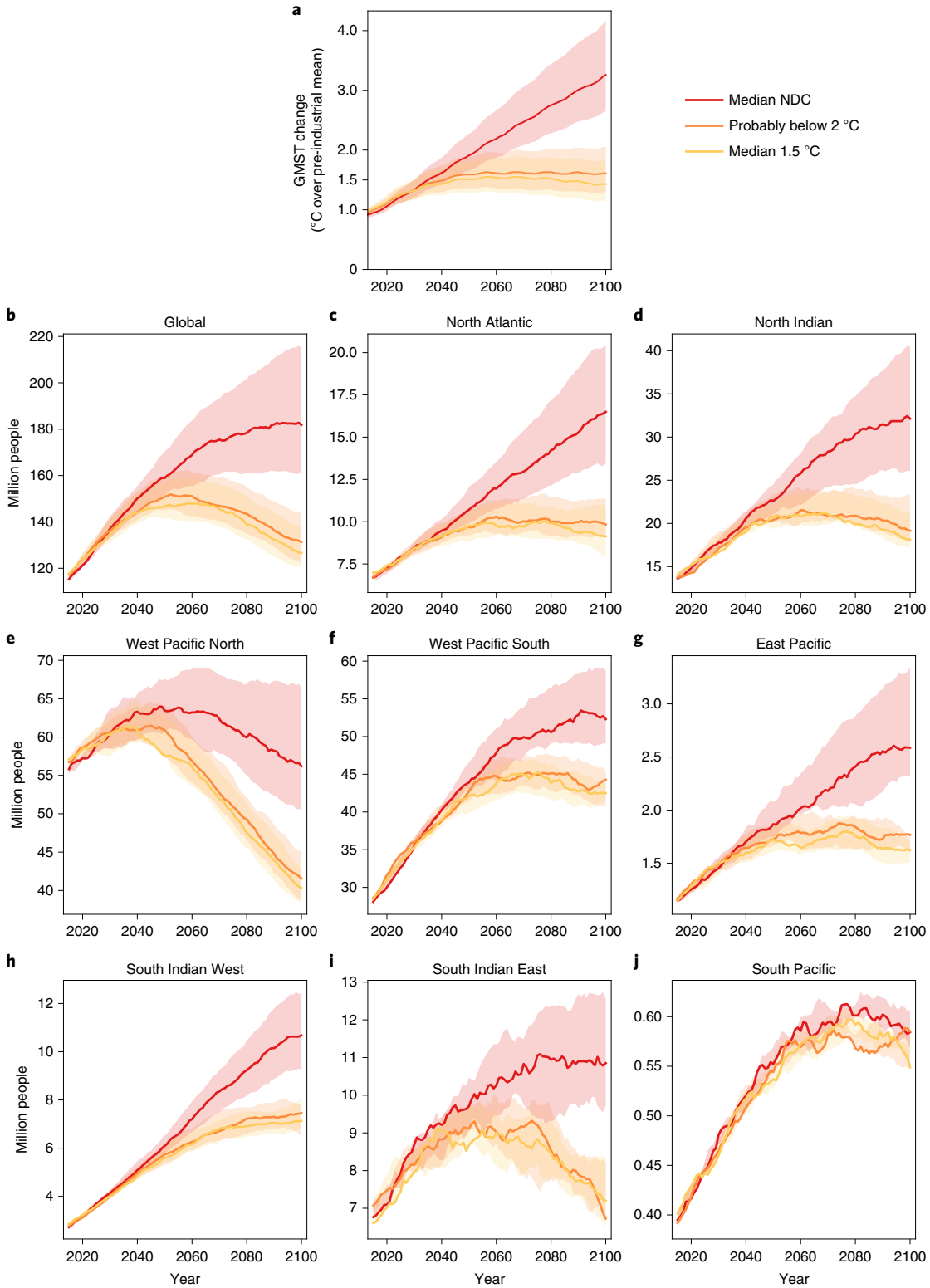

Fig. 3 | Future population exposure for different warming scenarios. a, GMST change under three warming scenarios. **b**–**j**, Projected population exposed to TCs annually for three warming scenarios (median NDC, red; probably below 2 °C, orange; and median GMST below 1.5 °C, yellow) and population development according to SSP2 until 2100. The solid lines represent 11-year running-mean exposure as given by the mean response across all four GCMs; the shaded regions correspond to the 66.7% confidence intervals due to NDC pathway and climate sensitivity uncertainty (see Methods for the details).

This purely intensity-driven increase is caused by intensifying TCs that exceed the threshold wind speed of 64 knots more often. Note that our definition of exposure does not reflect projected trends in impact severity, as intensity increases of TCs already stronger than the 64-knot threshold are not recorded explicitly, and TC impacts usually scale super-linearly with wind speed[17].

To analyse the temporal evolution of TC exposure under the joint forcing of climate change and socio-economic development,

we combine TC impacts at specific warming levels, extracted from the RCP6.0 scenarios, with population patterns from the Shared Socioeconomic Pathways (SSPs) for various base years according to SSP2. SSP2 represents a middle-of-the-road scenario in terms of economic and demographic development and in terms of climate change mitigation, and it is consistent with the current NDCs[24]. In terms of population growth, all SSPs (except SSP3) show a qualitatively similar development path with a peaking world population around mid-century and a decline thereafter (Supplementary Fig. 1), albeit with local differences related to urban sprawl. When analysing joint impacts of climate change and socio-economic development, the timing when certain warming levels are reached becomes crucial (Fig. 2). A 2 °C world in 2050 increases the baseline exposure (1 °C world with fixed 2015 population patterns) by 52 million people (+41%). Reaching 2 °C of global warming in 2080 or 2100 limits this number of people exposed to 40 million (+31%) and 25 million (+20%), respectively. While the effects of population growth and climate change would seriously amplify TC exposure in 2050, the opposite would be true in 2100, when a declining population in TC-prone areas would partially compensate for the additional exposure caused by warming (Fig. 2d). These findings are even more pronounced at the country level. In 2050 and at 2 °C of warming, all TC-prone countries are projected to see a rise in TC exposure with respect to their current baseline, with exposure changes of nearly 300% in some East African countries (Fig. 2a). Under less rapid warming scenarios, this picture changes: delaying 2 °C of warming to 2080 or 2100 would result in a reduction of exposed population in the Caribbean and in East Asia, in particular in Japan, China and the Korean peninsula. The reduced exposure in East Asia, causing most of the absolute projected decrease globally, overshadows the continuously growing exposure in other parts of the world. In particular, the United States, Oceania and East African countries are projected to see strong (by at least 100%) increases in TC exposure towards the end of this century, most likely also resulting in strong increases in TC damages in the United States as well as in poverty and (internal) migration in the other strongly affected regions. In agreement with a recent study, our tool also projects strong increases in TC exposure for the Arabian peninsula[25].

Finally, we demonstrate how the tool can be applied to derive exposure estimates for global warming pathways not originally covered by expensive GCM simulations. Our probabilistic TC tool is applied to study TC exposure for three alternate warming scenarios, again on the basis of population development according to SSP2: (1) an extended warming scenario according to current NDCs, (2) a scenario with GMST likely to be below 2 °C at the end of the century and (3) a scenario with a median GMST of 1.5 °C at the end of the century. These scenarios are chosen because they represent the spread between current best efforts and the ambitious targets of the Paris Agreement. To construct these temperature scenarios, we use the complexity-reduced Model for the Assessment of Greenhouse Gas Induced Climate Change (MAGICC 6.8) in the historically constrained probabilistic setup with 600 parameterizations[26] that requires emission scenarios as input. To obtain the temperature pathways for the 1.5 °C and 2 °C targets, we use readily available multi-gas scenarios, while the NDC pathway is a custom-mode scenario that extends current NDCs until 2100. We here rely on a medium-NDC case as the average between low and high 2030 emissions that were constructed for the Climate Action Tracker (CAT)[27]. The NDC scenario is then extended to 2100 using the constant quantile extension method[28] and translated to a temperature pathway using MAGICC. The extended NDC scenario reaches 2 °C of warming around mid-century, while the scenarios in line with the Paris Agreement (termed Paris scenarios in the following) never exceed 2 °C until the end of this century (Fig. 3a). The Paris scenarios project a peak in TC-exposed population of about 150 million people at mid-century (Fig. 3b), thereafter declining to exposure levels slightly higher than present-day values. In other words, the worst impacts will be over after 2050. In contrast, exposure according to the NDC scenario rises throughout the century, reaching annual TC exposure of about 180 million people at the end of the century. According to our tool, the annual difference in exposure between the NDC and Paris scenarios starts to diverge around 2030, already reaching an annual difference of 10 million exposed people by mid-century. This difference becomes even more pronounced when looking at the cumulative number of people exposed. Following a warming pathway that limits warming to 1.5 °C could reduce cumulative exposure by as much as 1.88 billion people by the end of this century compared with a pathway determined by the current NDCs. This global pattern is similarly observed for the various world regions (Fig. 3c–j). The northwestern Pacific (Fig. 3e) is the only region where all warming scenarios show a decline in exposure after mid-century (albeit with strongly differing trends), while in the southern Pacific (Fig. 3j), all warming scenarios display rather similar exposure patterns over time.

Discussion

TCs are among the costliest natural disasters worldwide, and their future impacts under the co-evolution of climate change and socio-economic development represent a societal challenge. The present analysis informs about future TC exposure at the country level and at different levels of warming. It quantifies TC exposure in terms of the (one-minute sustained) TC wind footprint reaching hurricane-force winds, thereby accounting for maximum wind speed and TC size but neglecting more turbulent wind properties such as gustiness and directional changes, as well as exposure duration. While the present exposure measure provides a very good first-order proxy of TC impacts in many situations, it might show limitations in others. TC properties might change with warming climate—for example, resulting in even longer exposure duration due to slower-moving or stalling TCs[11]. Also, TC damages derived from exposure in conjunction with vulnerability might be misrepresented. In this case, all wind-related components listed above have been shown to be important drivers of TC damages[29,30]. Interestingly, directional changes and duration have been shown to become less important for strong TC events[31], which cause most of the impact. Finally, wind exposure might be an improper proxy of exposure to TC co-hazards such as extreme precipitation or storm surges, which are not quantified here due to the computational challenges involved for a global study like ours. Water-related impacts through coastal and pluvial flooding can only be indirectly assessed via the TC wind footprint. Projected increases in heavier precipitation events[10] and stronger surges due to sea level rise[12] remain outside the scope of this assessment. Taken together, the impacts avoided in terms of wind exposure defined here very probably result in an even stronger benefit due to avoided water-related exposure and economic damages, which scale super-linearly with wind speed[17]. Moreover, relevant socio-economic impacts do occur below the hurricane strength threshold of 64 knots assumed here. The present assessment is therefore conservative, and the benefit of avoided exposure and damages might be much higher when including impacts from tropical storms (sustained wind speed above 33 knots).

In general, TC impacts caused by global warming in conjunction with socio-economic development show a strong and nonlinear path dependence. Path-dependent impacts are most likely universal and relevant for various climate extremes, such that the overall benefits of stringent climate action are expected to be much bigger. However, one question remains: how large is the negative feedback of climate extremes on socio-economic development pathways? Recent work suggests that slow-onset events may alter socio-economic development[32], but evidence from TC-related studies in the United States shows that the picture is more complex for rare and unanticipated extreme events. Here, long-term TC experience, the severity of TC

impacts and various socio-economic variables (for example, income perspectives) impede the prediction of future socio-economic development[33].

Online content

Any methods, additional references, Nature Research reporting summaries, source data, extended data, supplementary information, acknowledgements, peer review information; details of author contributions and competing interests; and statements of data and code availability are available at https://doi.org/10.1038/s41558-021-01157-9.

Received: 14 January 2020; Accepted: 19 August 2021;

References

1. Geiger, T., Frieler, K. & Bresch, D. N. A global historical data set of tropical cyclone exposure (TCE-DAT). *Earth Syst. Sci. Data* **10**, 185–194 (2018).
2. Berlemann, M. & Wenzel, D. Hurricanes, economic growth and transmission channels: empirical evidence for countries on differing levels of development. *World Dev.* **105**, 231–247 (2018).
3. Peduzzi, P. et al. Global trends in tropical cyclone risk. *Nat. Clim. Change* **2**, 289–294 (2012).
4. Estrada, F., Botzen, W. J. W. & Tol, R. S. J. Economic losses from US hurricanes consistent with an influence from climate change. *Nat. Geosci.* **8**, 880–884 (2015).
5. Bakkensen, L. A. & Mendelsohn, R. O. Risk and adaptation: evidence from global hurricane damages and fatalities. *J. Assoc. Environ. Resour. Econ.* **3**, 555–587 (2016).
6. Geiger, T., Frieler, K. & Levermann, A. High-income does not protect against hurricane losses. *Environ. Res. Lett.* https://doi.org/10.1088/1748-9326/11/8/084012 (2016).
7. Vecchi, G. A. et al. Tropical cyclone sensitivities to CO_2 doubling: roles of atmospheric resolution, synoptic variability and background climate changes. *Clim. Dyn.* **53**, 5999–6033 (2019).
8. Noy, I. The socio-economics of cyclones. *Nat. Clim. Change* **6**, 343–345 (2016).
9. Kummu, M. et al. Over the hills and further away from coast: global geospatial patterns of human and environment over the 20th–21st centuries. *Environ. Res. Lett.* https://doi.org/10.1088/1748-9326/11/3/034010 (2016).
10. Emanuel, K. Assessing the present and future probability of Hurricane Harvey's rainfall. *Proc. Natl Acad. Sci. USA* **114**, 12681–12684 (2017).
11. Kossin, J. P. A global slowdown of tropical-cyclone translation speed. *Nature* **558**, 104–107 (2018).
12. Woodruff, J. D., Irish, J. L. & Camargo, S. J. Coastal flooding by tropical cyclones and sea-level rise. *Nature* **504**, 44–52 (2013).
13. Kossin, J. P., Emanuel, K. A. & Vecchi, G. A. The poleward migration of the location of tropical cyclone maximum intensity. *Nature* **509**, 349–352 (2014).
14. Emanuel, K. Downscaling CMIP5 climate models shows increased tropical cyclone activity over the 21st century. *Proc. Natl Acad. Sci. USA* **110**, 12219–12224 (2013).
15. Bakkensen, L. A., Shi, X. & Zurita, B. D. The impact of disaster data on estimating damage determinants and climate costs. *Econ. Disasters Clim. Change* **2**, 49–71 (2017).
16. Gettelman, A., Bresch, D. N., Chen, C. C., Truesdale, J. E. & Bacmeister, J. T. Projections of future tropical cyclone damage with a high-resolution global climate model. *Climatic Change* **146**, 575–585 (2017).
17. Mendelsohn, R., Emanuel, K., Chonabayashi, S. & Bakkensen, L. The impact of climate change on global tropical cyclone damage. *Nat. Clim. Change* **2**, 205–209 (2012).
18. Strobl, E. The economic growth impact of natural disasters in developing countries: evidence from hurricane strikes in the Central American and Caribbean regions. *J. Dev. Econ.* **97**, 130–141 (2012).
19. Frieler, K. et al. Assessing the impacts of 1.5 °C global warming—simulation protocol of the Inter-Sectoral Impact Model Intercomparison Project (ISIMIP2b). *Geosci. Model Dev.* **10**, 4321–4345 (2017).
20. Aznar-Siguan, G. & Bresch, D. N. CLIMADA v1: a global weather and climate risk assessment platform. *Geosci. Model Dev.* **12**, 3085–3097 (2019).
21. *The Emissions Gap Report 2018* (UNEP, 2018).
22. Klein Goldewijk, K., Beusen, A., Doelman, J. & Stehfest, E. Anthropogenic land use estimates for the Holocene—HYDE 3.2. *Earth Syst. Sci. Data* **9**, 927–953 (2017).
23. Jones, B. & O'Neill, B. C. Spatially explicit global population scenarios consistent with the Shared Socioeconomic Pathways. *Environ. Res. Lett.* https://doi.org/10.1088/1748-9326/11/8/084003 (2016).
24. Riahi, K. et al. The Shared Socioeconomic Pathways and their energy, land use, and greenhouse gas emissions implications: an overview. *Glob. Environ. Change* **42**, 153–168 (2017).
25. Murakami, H., Vecchi, G. A. & Underwood, S. Increasing frequency of extremely severe cyclonic storms over the Arabian Sea. *Nat. Clim. Change* **7**, 885–889 (2017).
26. Meinshausen, M. et al. Greenhouse-gas emission targets for limiting global warming to 2 °C. *Nature* **458**, 1158–1162 (2009).
27. Rocha, M. et al. *Paris Agreement in Force, but No Increase in Climate Action* Tech. Rep. (Climate Action Tracker, 2016).
28. Gütschow, J., Jeffery, M. L., Schaeffer, M. & Hare, B. Extending near-term emissions scenarios to assess warming implications of Paris Agreement NDCs. *Earth's Future* **6**, 1242–1259 (2018).
29. Czajkowski, J. & Done, J. As the wind blows? Understanding hurricane damages at the local level through a case study analysis. *Weather Clim. Soc.* **6**, 202–217 (2014).
30. Zhai, A. R. & Jiang, J. H. Dependence of US hurricane economic loss on maximum wind speed and storm size. *Environ. Res. Lett.* https://doi.org/10.1088/1748-9326/9/6/064019 (2014).
31. Done, J. M., Simmons, K. M. & Czajkowski, J. Relationship between residential losses and hurricane winds: role of the Florida building code. *ASCE ASME J. Risk Uncertain. Eng. Syst. A* https://doi.org/10.1061/AJRUA6.0000947 (2018).
32. Rigaud, K. K. et al. *Groundswell: Preparing for Internal Climate Migration* (World Bank, 2018).
33. Fussell, E. et al. Weather-related hazards and population change. *Ann. Am. Acad. Polit. Soc. Sci.* **669**, 146–167 (2017).

Methods

Climate data. GMST and ENSO time series are extracted from the GCMs (HadGEM2-ES, MIROC5, IPSL-CM5A-LR and GFDL-ESM2M) that drive the dynamic TC model. The construction of synthetic future GMST series not covered by the RCPs and used for Fig. 3 is described below.

We extract annual absolute GMST on the basis of mean monthly temperature data (variable 'tas') from the respective GCMs for the piControl, historical (1861–2005), RCP2.6 (2006–2100 (2299 where required)) and RCP6.0 (2006–2100) runs from the Coupled Model Intercomparison Project Phase 5 (CMIP5) archive. We merge historical data with the respective RCP time series and apply a 21-year running mean for smoothing. Then, the smoothed absolute GMST time series are normalized such that relative GMST changes with respect to the average piControl GMST are equal to observed changes relative to the observed 1850–1900 GMST (in accordance with the Fifth Assessment Report (AR5) of the IPCC[34]). This corresponds to a shift in the relative GMST changes by the following values: −0.06 °C for HadGEM2-ES, 0.76 °C for MIROC5, 0.02 °C for GFDL-ESM2M and −1.73 °C for IPSL-CM5A-LR. This ensures that potential differences in TC activity between observations and simulations due to different relative warming levels are minimized.

The extracted ENSO time series is based on the Equatorial Southern Oscillation Index. Being a relative index based on sea level pressure differences at the Equator, it is independent of trends in the climate data and better represents the ENSO influence on both hemispheres. To obtain the ENSO time series, we extract mean monthly sea level pressure (variable 'psl') from the CMIP5 sources referred to above and calculate the normalized difference between the standardized anomalies averaged between 5° N–5° S, 80° W–130° W and 5° N–5° S, 90° E–140° E, following the definition used by the National Oceanic and Atmospheric Administration[35]. Finally, we smooth the monthly ENSO time series with a three-month running mean and determine the region-specific mean annual ENSO index on the basis of the seasonal TC activity in each ocean basin, noting that the annual ENSO index for regions in the southern hemisphere is based on monthly values from adjacent years.

Note that independence between GMST and ENSO time series is ensured by smoothing the time series at very different timescales, thereby erasing correlations between GMST and ENSO.

Hazard data. Historically observed TC tracks between 1950 and 2015 are based on the International Best Track Archive for Climate Stewardship (v.03r10)[36], while the simulated TC tracks for the historical and future periods are taken from the archive provided by ISIMIP[19]. Note that ISIMIP provides the TC simulations only for research purposes and upon reasonable request. The ISIMIP archive contains simulated TC tracks that are generated using a dynamical downscaling model[14], which has been shown to reproduce the observed spatial and seasonal variability of TCs and trends in storm frequency around the globe[37]. The TC model is driven by climate input data from four different GCMs (HadGEM2-ES, MIROC5, IPSL-CM5A-LR and GFDL-ESM2M) provided by ISIMIP for the historical period (until 2005) and two RCP scenarios (RCP2.6 and RCP6.0) from 2006 onwards. The number of simulated years varies depending on the GCM due to available climate variables in the CMIP5 archive and constraints of the ISIMIP simulation protocol (1950–2100 (RCP2.6 and RCP6.0) for HadGEM2-ES, 1861–2299 (RCP2.6) and 1861–2100 (RCP6.0) for MIROC5, 1861–2299 (RCP2.6) and 1861–2100 (RCP6.0) IPSL-CM5A-LR, and 1861–2100 (RCP2.6 and RCP6.0) for GFDL-ESM2M). The corresponding RCP scenarios extend the historical scenario after 2005 and are jointly referred to as warming scenarios below. For each simulated year, 300 TCs are generated by randomly seeding a very large number of potential TC seeds. According to the boundary conditions prescribed by the driving GCM (for example, water temperatures and wind shear), only a very small fraction of the initial seeds intensify to become TCs, which are propagated forwards using a beta-and-advection model driven by winds derived from the GCMs[14]. The annual TC frequency for each simulated year is then determined by the fraction of initial seeds and the actually generated number of 300 annual events, upon multiplying with a single constant so that the global number of events since 1950 matches observations.

Processing hazard data. The TC track data (observations and simulations) are processed with a windfield model[38] to produce TCs with realistic size and intensity distributions according to the methodology used to produce the Tropical Cyclone Exposure Database[1] on a global spatial grid with 0.1° × 0.1° resolution. The windfield model accounts for individual TC sizes via the TC's radius of maximum winds, its intensity (via the minimum central pressure), its path (via latitude) and its translation speed (TC asymmetry) (see the following link for a visualization of an exemplary track: https://vimeo.com/352796694). Applying the same methodology for observations and simulations allows for a globally and historically consistent comparison of TC exposure. Next, the full sample of observed and simulated TC windfield data is reduced to contain landfalling events only, where we define landfall in terms of exposure—that is, given a minimum wind speed of more than 33 knots above land. For each of the eight world regions considered (East Pacific, North Atlantic, North Indian, South Indian East, South Indian West, West Pacific North, West Pacific South and South Pacific) (Fig. 1a), we then produce annual landfall time series for TC frequency (that is, the annual number of landfalls) and intensity (that is, the mean annual maximum wind speed at landfall). For the southern hemisphere, where TC seasons range across two years, effective annual time series are created by shifting the time stamp to cover a complete season and dropping incomplete seasons from the analysis. TC landfalls are recorded only once per region where wind speed at landfall is at its maximum. The observational landfall time series are used to calibrate the simulated landfall time series, as the provided TC simulations are not calibrated for this purpose. To do so, the total number of simulated landfalls and the mean annual wind speed at landfall per region between 1950 and 2015 (1980–2015 for North Indian, South Indian East, South Indian West and South Pacific due to the limited reliability of observations before the satellite era) are matched with observations. This provides a long-term average calibration of the hazard in physical terms (not in terms of exposure) that conserves fluctuations around the long-term mean caused by natural variability and stochasticity of landfall occurrence.

To analyse how the frequency and intensity of the simulated regional TC landfall time series (for each GCM–RCP combination) vary with GMST change and ENSO variability, we regress the respective time series with extracted GMST and ENSO data ('Climate data'). Correlations between GMST and ENSO time series are avoided by using a 21-year running mean for GMST and a three-month running mean for ENSO. Frequency is regressed using Poisson regression, which is better suited for count data than linear regression[39]; intensity is regressed using ordinary least squares. We use a hierarchy of regressions to eliminate insignificant contributions, whose presence might alter the significance of the remaining climate indices. Depending on the region–GCM combination, a substantial fraction of landfall variability can be explained by GMST and ENSO, in particular for landfall frequency (see Supplementary Tables 1 and 2 for lists of regression statistics for frequency and intensity, respectively). The remaining residual (or unexplained) variance is explicitly accounted for in the development of the probabilistic TC tool in the following step.

Emulating impact time series. On the basis of the functional dependence of the simulated TC landfall time series and GMST and ENSO retrieved above, we now construct a probabilistic tool. This tool allows us to draw a large number of random TC samples that mimic the number of TC landfalls and mean landfall intensity in a given region and year (with a given GMST and ENSO state). We refer to a TC sample as a full set of TCs with landfall that could potentially occur in a given region and year. These samples are drawn from all available simulated TCs with landfall for a given GCM and warming scenario in two steps. First, a random sample without replacement of TCs by region is drawn according to a Poisson distribution with the expected number of landfalls prescribed by the functional GMST and ENSO dependence. Second, the mean landfall intensity of this sample is compared to the expected mean landfall intensity. If the mean landfall intensity does not fall into the interval given by the expected mean landfall intensity and the residual variation obtained from the intensity regression mentioned above, the random sample is rejected, and a new sample is drawn in step 1. If repeatedly no representative sample can be drawn, the set of all landfalling TCs is iteratively and randomly reduced by an increasing fraction of events with landfall speeds above (below) the expected mean landfall speed until the desired number of random TC samples for a given year (with a given GMST and ENSO state) are obtained. For the present work, we generated 100 TC samples (that is, 100 full artificial TC seasons) for each year, basin, GCM and warming scenario. This results in a total of 1,712,000 random TC samples that were analysed for Fig. 1. When applying the probabilistic tool to produce Figs. 2 and 3, only the warming scenario according to RCP6.0 was used due to almost identical scaling of the two warming scenarios (RCP2.6 and RCP6.0; Fig. 1).

Note that Figs. 1–3 and Extended Data Figs. 1 and 2 show results irrespective of ENSO states—that is, the results presented in the manuscript are a superposition of negative, positive and neutral ENSO phases. This is due to the fact that ENSO is not very consistently represented across the GCMs used in our analysis, and we were thus unable to identify a relevant ENSO signal in our multi-model results.

To disentangle future hazard trends into respective intensity and frequency contributions, we additionally create random TC samples where the frequency change with GMST is fixed at 1 °C of warming (Extended Data Fig. 2). We use the median annual frequency determined from the GMST interval 0.5 °C–1.5 °C for each basin, GCM and warming scenario to obtain the expected number of landfalls drawn from a Poisson distribution for all years where the GMST change is larger 1 °C (see step 1 above).

Socio-economic data. We use gridded population data available through the ISIMIP project[19] with a spatial resolution of 0.1° × 0.1° (360 arcsec) from 1950 to 2100. The historical data are based on the HYDE population data[22] and upscaled from the original 300-arcsec resolution. Future gridded population data that are both quantitatively and qualitatively consistent with SSP2 (ref. [23]) are downscaled from their original 450-arcsec resolution. After 2005, the historical data are linearly merged to match the SSP2 data in 2010.

Impact assessment. In this study, a population is defined as exposed once the grid cell hosting the population experiences a minimum wind speed of 64 knots.

Additional exposure due to multiple TCs affecting the same grid cell in the same year is counted additionally (double counting). The exposed population is then aggregated to the country, regional or global level. This procedure is conducted for observed exposure and each of the 100 random TC samples for each year. As output, we analyse the statistical mean as well as the 66.7% confidence interval.

Population values can be fixed to desired reference years (for example, 2015) to analyse the differential impacts of climate change and socio-economic development separately. The differential impact of one degree of additional warming (±0.2 °C interval) with respect to the baseline (2015 at 1 °C) for different future years X is calculated as the mean change for identical warming levels in different years (that is, soc = 0.5 × (soc$X$ at 1 °C − soc2015 at 1 °C + soc$X$ at 2 °C − soc2015 at 2 °C) and for different warming levels in identical years (that is, cc = 0.5 × (cc$X$ at 2 °C − cc$X$ at 1 °C + cc2015 at 2 °C − cc2015 at 1 °C) (Fig. 2). The baseline and the joint effect of climate change and socio-economic development (cc + soc) are respectively determined as the exposure in 2015 at 1 °C and in year X at 2 °C. The difference between cc + soc and the baseline also determines the relative change at the country level (Fig. 2).

Using synthetic GMST time series not covered by the RCPs (for example, as determined by the NDCs) in conjunction with the SSP2 development pathway allows us to capture arbitrary TC exposure trajectories (Fig. 3 and the discussion below).

Note that the impacts at different GMST levels cannot be generalized to GMST or sea-surface temperature changes caused by other processes such as natural climate variations or aerosol-induced climate change, as these may be unrelated to GMST trends caused by GHGs.

Calibration, validation and uncertainty assessment. Here, physical properties of TCs at landfall are used to calibrate simulated TC exposure with observations. We refrain from using population exposure for calibration and are also reluctant to use population exposure for validation, as historical exposure represents just one realization of potential TC exposure and is therefore intrinsically uncertain. The calibration method using physically based long-term regional TC landfall statistics, as discussed above, represents the least limiting way. We verified that despite these modest constraints, the simulated distribution of annually exposed population agrees very well with observations (Extended Data Fig. 1). Uncertainty in exposure is assessed by analysing the GCM-specific 100-sample mean exposure and its 66.7% confidence interval for each simulated GMST value (Fig. 1). Globally and for all regions except South Indian East, we find that the observed long-term mean (and the 66.7% range of interannual variability) of observed population exposure agrees very well with the estimates of the probabilistic tool. The differences in observed and simulated exposure, in particular for South Indian East, are most likely caused by simulated TCs that reach very close to the Equator and therefore affect some regions that are less affected in observations. Similarly, we observe that some simulated TCs reach too far north (south) in the northern (southern) hemisphere. Restricting TC exposure to wind speeds of at least 64 knots, as we do here, reduces such artefacts to a minimum.

For Fig. 2, we consider multi-GCM mean exposure, on the basis of the GCM mean conducted across all years (with 100 random TC samples per year) that coincide with the considered warming level ±0.2 °C. Country-specific trends in exposure (Fig. 2a–c) are considered to be significant if at least three out of four models agree on the sign of the change (non-hatched); the ranges for GCM-specific model realizations are displayed in Fig. 2d in addition to the multi-GCM mean.

The 66.7% confidence interval of the temperature projections stems from the climate system simulation only and does not include the uncertainty of the NDC quantification or the pathway extension (Fig. 3a). Similarly, the uncertainty of the corresponding population exposure trajectories (Fig. 3b–j) is based on the uncertainty of the climate system simulation only.

NDC quantification. The analysis in Fig. 3 is based on a medium-NDC case as the average between low and high 2030 emissions. The high and low cases are both constructed as the mean of the CAT's[27] and NDC factsheet's[40] high and low values. Averaging is done on aggregate values for the IPCC's RC5 regions[41] (page 1287) and emissions including land use, land use change and forestry (LULUCF). Emissions from international shipping and aviation (bunkers) are not covered by the NDCs and have to be added to the NDC emissions levels. We take the global 2030 values from CAT and distribute them over the five regions using the 2014 regional shares of CO_2 bunker emissions from the CDIAC 2017 release[42]. Our NDC quantification amounts to 2030 emissions of 55.6 $GtCO_2e$ (including emissions from international transport and land use).

Extending the NDC scenarios to 2100. The NDC scenarios are extended to 2100 using the constant quantile extension method[28]. This method is based on the idea that after the end of the NDC period, climate policy is continued at a similar level of effort relative to scenarios in a scenario database. Here, we use the scenario database of the IPCC's AR5 (ref. [43]), which is harmonized to historical emissions from PRIMAP-hist v.1.2 (refs. [44,45]). The database is filtered to remove scenarios not fitting the assumption of a continued level of effort in climate policy. We filter out the IPCC AR5 policy classes P3 and P4, which describe scenarios where serious climate action only starts after 2030, as well as the negative emissions class N2 scenarios (which have negative emissions exceeding 20 Gt per year). We also remove the GCAM EMF27 mitigation scenarios and the GCAM LIMITS 450 ppm and 500 ppm scenarios, as they show negative total emissions for R5LAM and/or R5MAF before 2040 with emissions rising afterwards, which is problematic for the pathway extension methods and contrary to the idea of continuation of climate policy at a similar level of ambition. After the filtering process, the scenarios are binned according to the 'climate', 'technology' and 'model' parameters from the AR5DB such that all models that share the same values for the three parameters are grouped. The models are then weighted such that each group collectively has a unit weight of one. These weighted pathways are used to calculate a scenario distribution. The NDC pathway is compared to this distribution, and its quantile within the distribution in the NDC target year (2030) is determined. The extended pathway is constructed by following this quantile through the scenario distribution until 2100. This method is preferred because it conserves the level of climate policy in the NDCs for the extension of the scenario, while other approaches (for example, using a fixed scenario or constant emissions for the extension) use a prescribed future level of climate policy. The continuation of climate policy at a similar level of effort thus provides a reasonable middle-of-the-road option that assumes neither a reversal of climate policies nor a sudden increase in ambition. For more details on the method and the comparison of different methods to extend NDC pathways, see refs. [28,46].

Calculating corresponding GMST pathways. We use MAGICC v.6.8 in the historically constrained probabilistic setup with 600 parameterizations[26]. The period for the historical constraint is 1986–2005. To obtain the GMST anomaly towards the historical period of 1850–1900, we add 0.61 °C to the result relative to 1986–2005 (ref. [34], page 193). The climate sensitivity distribution is taken from ref. [47]. As this method needs a separate LULUCF time series, we subtract the CAT LULUCF NDC time series from the output of the pathway extension methodology and use the LULUCF time series together with the obtained pathway excluding LULUCF as input.

To obtain GMST pathways for the 1.5 °C and 2 °C targets, we use readily available multi-gas scenarios. The 2 °C pathway is RCP2.6 and remains below 2 °C with 66% probability, while the 1.5 °C pathway is a scenario that has a median warming of below 1.5 °C. The median temperature of these pathways differs by less than 0.2 °C because 2 °C is avoided with at least 66% probability, while 1.5 °C is avoided with at least 50% probability (Fig. 3a).

Data availability

The historical[48] and future[49] population data are freely available online. The historical TC exposure data are available from the Tropical Cyclone Exposure Database archive[50]. The TC track simulations are available for scientific purposes only and upon request from WindRiskTech (info@windrisktech.com). Requests regarding the CLIMADA impact model should be addressed to D.N.B. (dbresch@ethz.ch). The data to display country outlines and coastlines are based on the Generic Mapping Tools[51]. All remaining data that support the findings of this study are available from the corresponding author upon request.

Code availability

The simulations to quantify the TC impact were conducted using the Python tool CLIMADA, available at https://github.com/CLIMADA-project/climada_python/releases/tag/v2.2.0. In particular, the tool to generate the artificial TC exposure time series is freely available at https://github.com/CLIMADA-project/climada_petals/blob/main/doc/tutorial/climada_hazard_emulator.ipynb. The model to generate the TC tracks, the model to construct the temperature scenarios (MAGICC 6.8 and the climate module of the Potsdam Real-Time Integrated Model for the probabilistic assessment of emission paths (PRIMAP)) and the PRIMAP emissions module used for the creation and extension of the NDC pathways are proprietary and cannot be shared publicly. All remaining code that was used to analyse the data and produce the figures is available from the corresponding author upon request.

References

34. IPCC *Climate Change 2013: The Physical Science Basis* (eds Stocker, T. F. et al.) (Cambridge Univ. Press, 2013).
35. *Equatorial Southern Oscillation Index (ESOI)* (NOAA, 2019); https://www.cpc.ncep.noaa.gov/products/analysis_monitoring/bulletin_tmp/figt2.shtml
36. Knapp, K. R., Kruk, M. C., Levinson, D. H., Diamond, H. J. & Neumann, C. J. The International Best Track Archive for Climate Stewardship (IBTrACS) unifying tropical cyclone data. *Bull. Am. Meteorol. Soc.* **91**, 363–376 (2010).
37. Emanuel, K., Sundararajan, R. & Williams, J. Hurricanes and global warming: results from downscaling IPCC AR4 simulations. *Bull. Am. Meteorol. Soc.* **89**, 347–367 (2008).
38. Holland, G. A revised hurricane pressure–wind model. *Mon. Weather Rev.* **136**, 3432–3445 (2008).
39. Dobson, A. J. *An Introduction to Generalized Linear Models* (Chapman & Hall/CRC, 2002).

40. Meinshausen, M. & Alexander, R. *NDC and INDC Factsheets.* November 2016 version *(*Australian-German Climate and Energy College, The University of Melbourne, 2016).
41. IPCC *Climate Change 2014: Mitigation of Climate Change* (eds Edenhofer, O. et al.) (Cambridge Univ. Press, 2014).
42. Boden, T. A., Andres, R. J. & Marland, G. *Global, Regional, and National Fossil-Fuel CO2 Emissions (1751 - 2014) (V. 2017)* (Carbon Dioxide Information Analysis Center, Oak Ridge National Laboratory, 1999); https://doi.org/10.3334/CDIAC/00001_V2017
43. IPCC *Climate Change 2014: Impacts, Adaptation, and Vulnerability* (eds Field, C. B. et al.) (Cambridge University Press, 2014).
44. Gütschow, J., Jeffery, M. L., Gieseke, R. & Gebel, R. *The PRIMAP-hist National Historical Emissions Time Series (1850–2015)* v.1.2 (GFZ Data Services, 2018).
45. Gütschow, J. et al. The PRIMAP-hist national historical emissions time series. *Earth Syst. Sci. Data* **8**, 571–603 (2016).
46. Jeffery, M. L., Gütschow, J., Rocha, M. R. & Gieseke, R. Measuring success: improving assessments of aggregate greenhouse gas emissions reduction goals. *Earth's Future* **6**, 1260–1274 (2018).
47. Rogelj, J., Meinshausen, M. & Knutti, R. Global warming under old and new scenarios using IPCC climate sensitivity range estimates. *Nat. Clim. Change* **2**, 248–253 (2012).
48. Klein Goldewijk, C. G. M. *Anthropogenic Land-Use Estimates for the Holocene: HYDE 3.2* (DANS, 2017); https://doi.org/10.17026/dans-25g-gez3
49. Jones, B. & O'Neill, B. C. *Global Population Projection Grids Based on Shared Socioeconomic Pathways (SSPs), 2010–2100* (NASA Socioeconomic Data and Applications Center, 2017); https://doi.org/10.7927/H4RF5S0P
50. Geiger, T., Frieler, K. & Bresch, D. N. *A Data Collection of Tropical Cyclone Exposure Data Sets (TCE-DAT)* (GFZ Data Services, 2017); https://doi.org/10.5880/pik.2017.011
51. Wessel, P. et al. The Generic Mapping Tools version 6. *Geochem. Geophys. Geosyst*. https://doi.org/10.1029/2019GC008515 (2019).

Acknowledgements

We thank T. Vogt for his valuable contribution to reworking the emulator code and making it publicly available. We further thank the ISIMIP team for their support. T.G. acknowledges funding through the framework of the Leibniz Competition SAW-2016-PIK-1 (ENGAGE) and funding by the German Federal Ministry of Education and Research (BMBF) project FKZ:01LA1829A (SLICE). K.F. acknowledges funding for ISIMIP through the BMBF for research projects 01LS1201A2 (ISIMIP2b) and 01LS1711A (ISIpedia). J.G. acknowledges support from the German Federal Ministry for the Environment, Nature Conservation and Nuclear Safety (16_II_148_Global_A_IMPACT) and from the BMBF (01LS1711A). The content and views presented in this paper are solely those of the authors and do not necessarily represent the views of Deutscher Wetterdienst (DWD).

Author contributions

T.G. and K.F. conceived and designed the research. K.E. generated the TC simulations. D.N.B. conducted the impact simulations. J.G. provided the future warming scenarios. T.G. developed the software tool and analysed and interpreted the data with help from all authors. All authors contributed to the writing of the manuscript.

Competing interests

The authors declare no competing interests.

Additional information

Extended data is available for this paper at https://doi.org/10.1038/s41558-021-01157-9.

Supplementary information The online version contains supplementary material available at https://doi.org/10.1038/s41558-021-01157-9.

Correspondence and requests for materials should be addressed to Tobias Geiger.

Peer review information *Nature Climate Change* thanks Cindy Bruyère, Ilan Noy and the other, anonymous, reviewer(s) for their contribution to the peer review of this work.

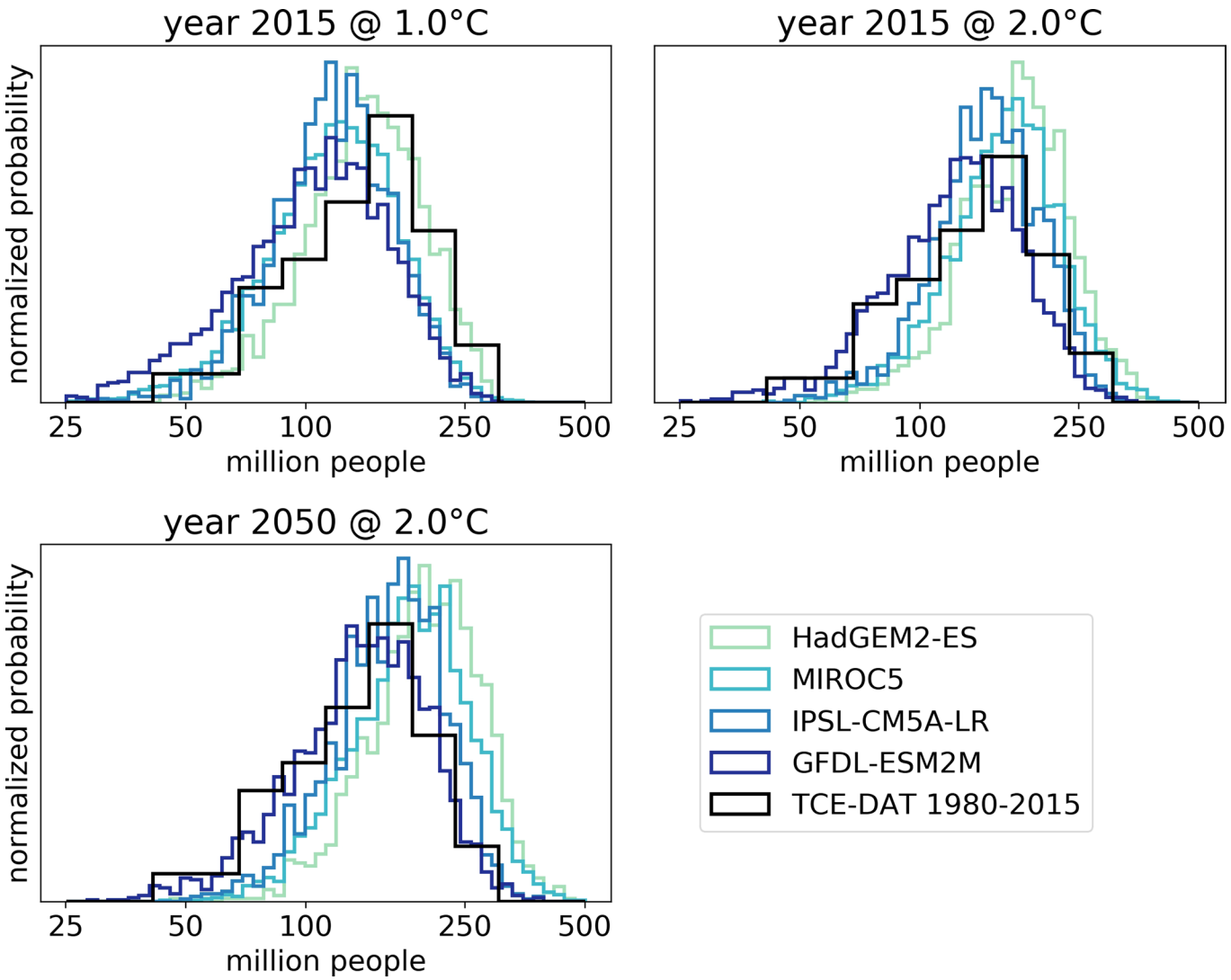

Extended Data Fig. 1 | Normalized distribution of global annually exposed population from tropical cyclones. The distributions are shown for two GMST levels (1 °C and 2 °C) and two fixed population patterns (2015 (observed) and 2050 (SSP2)) for modeled exposure (colored lines) based on RCP6.0 simulations compared to 1980–2015 observed exposure (black line). The logarithm of annual exposed population is binned for the observations (36 years, 12 bins) and for the simulations for all years falling in a 0.5 °C temperature interval around the desired GMST value (50 bins).

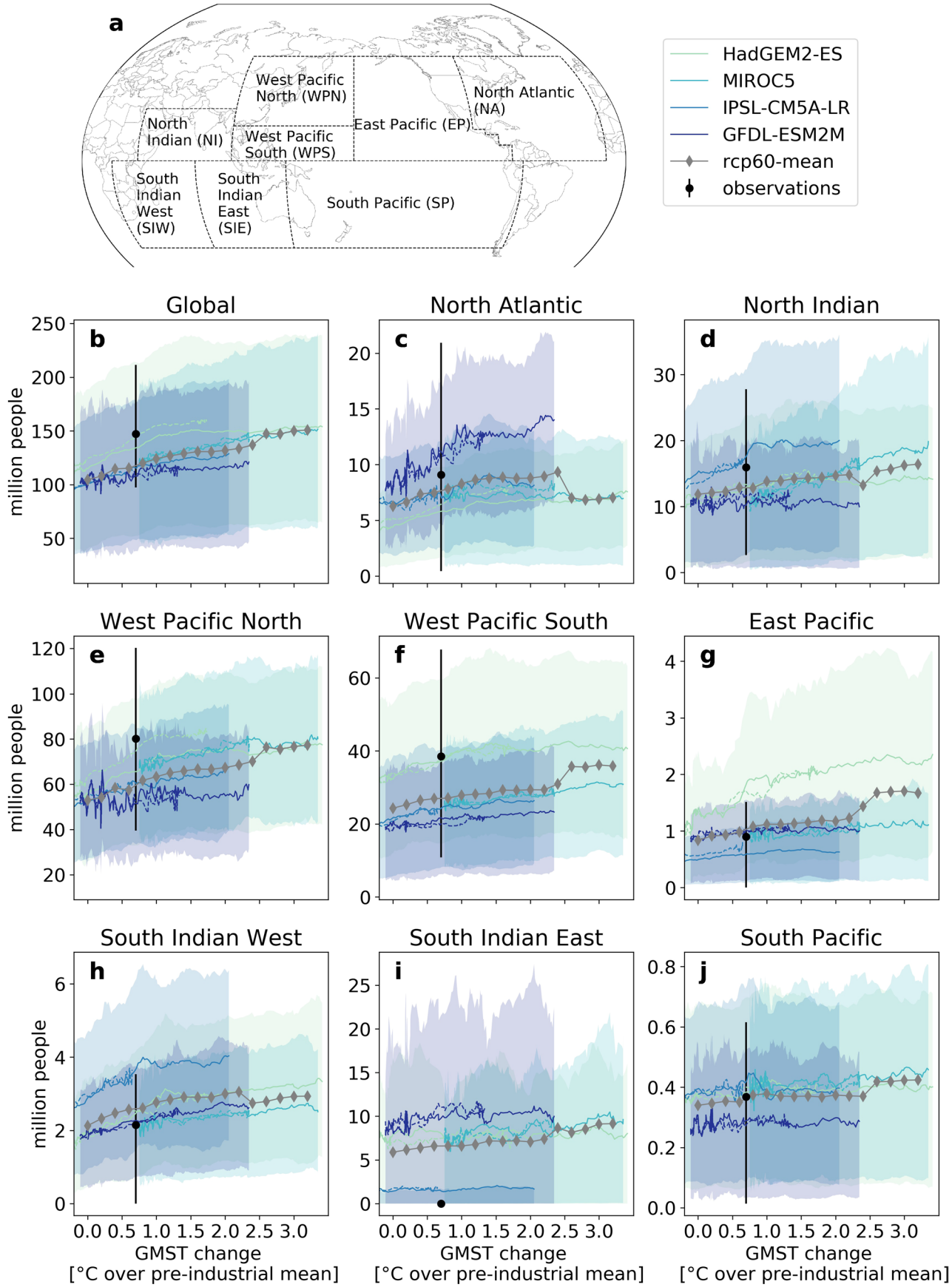

Extended Data Fig. 2 | Annual population exposure with global mean surface temperature (GMST) for constant tropical cyclone frequency. Same as Fig. 1 but with fixed TC frequency at 1°C of warming compared to the pre-industrial level.